JOURNAL OF MATERIALS SCIENCE 20 (1985) 4413–4420

Real time small-angle X-ray scattering from polystyrene crazes during fatigue

PETER J. MILLS, EDWARD J. KRAMER
Department of Materials Science and Engineering and the Materials Science Center, Cornell University, Ithaca, New York, USA

HUGH R. BROWN
IBM Research Laboratory, 5600 Cottle Road, San Jose, California, USA

Real time small-angle X-ray scattering (SAXS) from polystyrene (PS) crazed in cyclic three-point bending is investigated using intense X-ray radiation from the Cornell High Energy Synchrotron Source, CHESS. The SAXS patterns are recorded using a two-dimensional image intensifier/TV camera/video tape recorder system, operating at 30 frames/sec. At the maximum of the load cycle the SAXS pattern has a well defined streak normal to the craze fibrils. During the unloading portion of the cycle, however, the streak decreases in intensity and is spread into a diffuse fan. The loss of intensity is due to the decrease in volume of craze matter in the beam as the craze closes while the spreading of the diffraction pattern is due to the disorientation of the craze fibrils as they buckle in response to compression by the surrounding polymer matrix. Whilst reloading of the sample causes a relatively narrow SAXS streak to reappear, at the maximum load irreversible changes occur in the pattern from one cycle to the next. These changes are due to both an increase in craze fibril volume in the beam (craze growth) and to fibril breakdown and permanent disorientation.

1. Introduction

Both the fracture mechanics and mechanisms of crack growth during the fatigue of glassy polymers has received considerable attention [1–6]. However, little is known about the failure of the crazes which in unnotched specimens are the precursors to the crack. The optical interference technique [7], while useful for measuring the craze thickness and micromechanics at crack tips, does not have the necessary resolution to yield information on the craze microstructure. Transmission electron microscopy (TEM), while excellent for observing crazes under static loads, is not suitable for dynamic and fatigue studies owing to its requirements for thin film samples. It has been shown previously [8] that small-angle X-ray scattering (SAXS) can be used to investigate the craze microstructure of loaded and unloaded crazes. However, it has proved impossible to make SAXS measurements under dynamic conditions due to the low intensity of conventional X-ray sources.

With the advent of synchrotron hard X-ray sources such as CHESS, the Cornell High Energy Synchrotron Source, and SSRL, the Stanford Synchrotron Radiation Lab, this restriction no longer exists. What makes synchrotron radiation especially attractive for small-angle scattering is that it is already highly collimated (the angular divergence in the vertical plane at CHESS is < 0.1 mrad) so that relatively little attenuation takes place during collimation. The resulting usable flux is over four orders of magnitude greater than conventional X-ray sources. Synchrotron radiation has been used previously to undertake a preliminary investigation of craze initiation using a one-dimensional detector [9], but, as will become clear below, a

0022–2461/85 $03.00 + .12

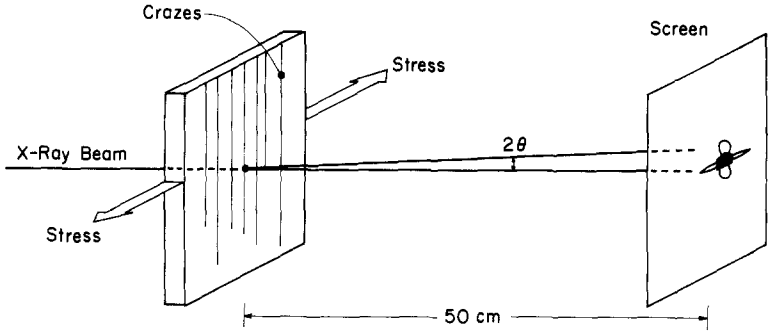

Figure 1 Schematic of the geometry of the SAXS experiment.

complete study of SAXS during fatigue will require a two-dimensional detector system such as that employed here.

SAXS studies, in common with other diffraction methods, do suffer from the disadvantage that all phase information is lost. Reconstruction of the scattering microstructure is difficult without prior knowledge of qualitative features of the craze structure. As a result, whilst transmission electron microscopists generally agree on the qualitative features of craze microstructure, one finds widely diverging models of this microstructure in the SAXS literature [8–18], and correspondingly large differences in craze parameters extracted from these models. In this work we will adopt the generally accepted model of craze microstructure constructed from TEM observations [19–24], namely that this microstructure consists of craze fibrils of highly oriented polymer (minority phase) embedded in a continuous void matrix (majority phase). Although interconnecting crosstie fibrils may be present, the main load bearing fibrils are highly oriented along the direction of maximum principal stress.

In our scattering geometry, shown in Fig. 1, the SAXS pattern from crazes consists of a cross through the origin. A typical pattern is shown in Fig. 2. An intense streak is observed which is parallel to the craze fibrils and normal to the craze surfaces (horizontal in Fig. 2). A less intense streak is seen normal to the fibrils and parallel to the craze surfaces (vertical in Fig. 2). The former streak is a rod in reciprocal space and is a result of external reflection from the craze surfaces [8, 17], whilst the latter streak, a disc in reciprocal space, represents the small-angle diffraction of the fibrils from which their

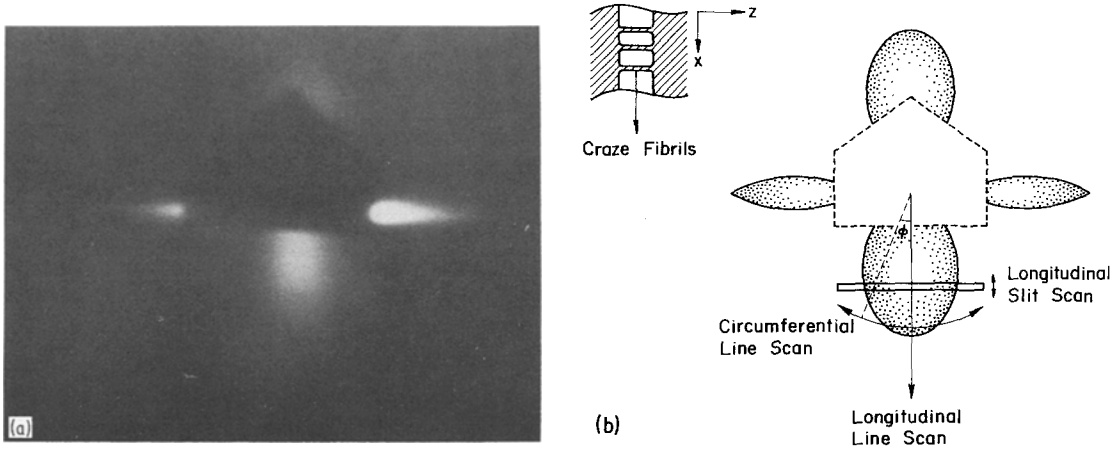

Figure 2 A typical SAXS pattern from crazes in a PS sheet under load. The insert shows the orientation of the craze fibrils which give rise to the vertical (x-axis) fibril scattering streak. Longitudinal and circumferential line scans have the geometry shown, while the slit scan is performed by translating the slit shown along the x-axis. Because of the asymmetric parasitic scattering from the Kratky collimator the beam stop is elongated in the negative x-direction. Only the fibril scattering in the positive x-direction is analysed.

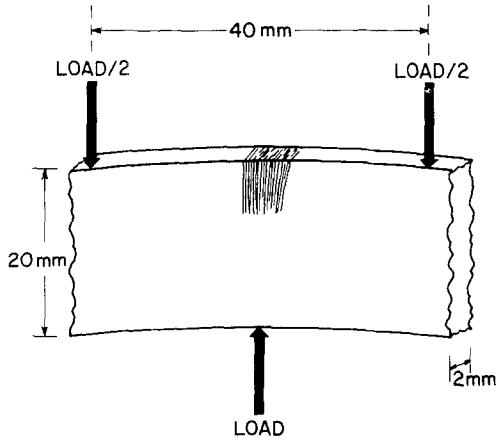

Figure 3 Loading geometry and craze morphology in the three-point bend test.

diameter, spacing and orientation can be computed. This initial report will be concerned only with the fibril scattering.

2. Experimental details

Sheets of commercial PS approximately 2 mm thick were cut into 60 mm × 20 mm strips. The samples were pre-crazed under three-point bending, as shown in Fig. 3. As a result a bundle of crazes grew only from flaws at the upper surface of the beam, the surface which was under tension. The present experimental apparatus afforded no means of directly measuring load but relative values may be inferred from the surface tensile strain computed from the applied displacement. The maximum strain which was imposed on this surface was 3.0% and the minimum 0.3%. Two types of test were conducted.

1. Stepwise loading and unloading with displacement step functions.
2. Cyclic loading at a frequency of 0.6 Hz with a triangular displacement waveform.

All testing was done at room temperature.

Monochromatic 8 keV X-rays (wavelength $\lambda = 0.154$ nm) from CHESS, with an approximate intensity of 2×10^{10} photons $mm^{-2} sec^{-1}$, were collimated using a Kratky collimator fitted with a 60 μm high entrance slit, the beam being narrowed to 2 mm in the horizontal direction. The detector system consisted of a thin ZnS(Ag) fluorescent screen coupled by fibre optics to a 40 mm diameter, three-stage Varo image intensifier. The resultant visible image was lens coupled to a vidicon camera, whose output could be simultaneously recorded and displayed on a CRT monitor. This system enables two-dimensional X-ray scattering patterns to be recorded and viewed at 525 lines/frame and 30 frames/sec.

The recorded frames were then processed using the Grinell image analysing system, Model GMR-274. This system is capable of digitizing a 480 × 512 array in real time. The digitized array can then be manipulated to average successive frames, enlarge certain areas, enhance black and white contrast and produce pseudo-colour mapping. Line scans of various geometries may also be performed. Two such scans were performed on the patterns shown here, a longitudinal scan along the centre line of the fibril scattering streak and a circumferential scan along a circle centred on the incident beam spot. The geometry of these scans is shown in Fig. 2b. In addition, the intensity captured by a slit placed perpendicular to the fibril streak and scanned along it (parallel to the centre line of the streak) was computed.

3. Results and discussion

After the PS bar was crazed by loading monotonically to the maximum load, SAXS patterns were recorded as it was unloaded in steps, the strain being maintained at each step for 10 sec. Unloading of the sample dramatically alters the fibril scattering as can be seen qualitatively in Fig. 4. As the strain, and hence the load, is reduced there is a decrease in intensity of the fibril scattering and a splaying and broadening of the streak. Fig. 5 shows the angular dependence of the fibril scattering intensity as measured with a longitudinal line scan, a single pixel element wide, at various steps in such an unloading sequence.

The decrease in intensity during unloading can be interpreted as a decrease in the total craze volume, V, in the beam as a result of reduced separation of the craze–bulk interfaces [25, 26]. Changes relative to the loaded state may be interpreted quantitatively since there must be a corresponding increase in the volume fraction, v_f, of fibrils in the craze, because the volume of fibrils, $v_f V$, in the craze remains constant during the unloading. We define the magnitude of the scattering vector $s = 2 \sin(\theta)/\lambda$, where 2θ is the scattering angle. The total slit smeared intensity of the fibril scattering is denoted by $i(s)$ and is

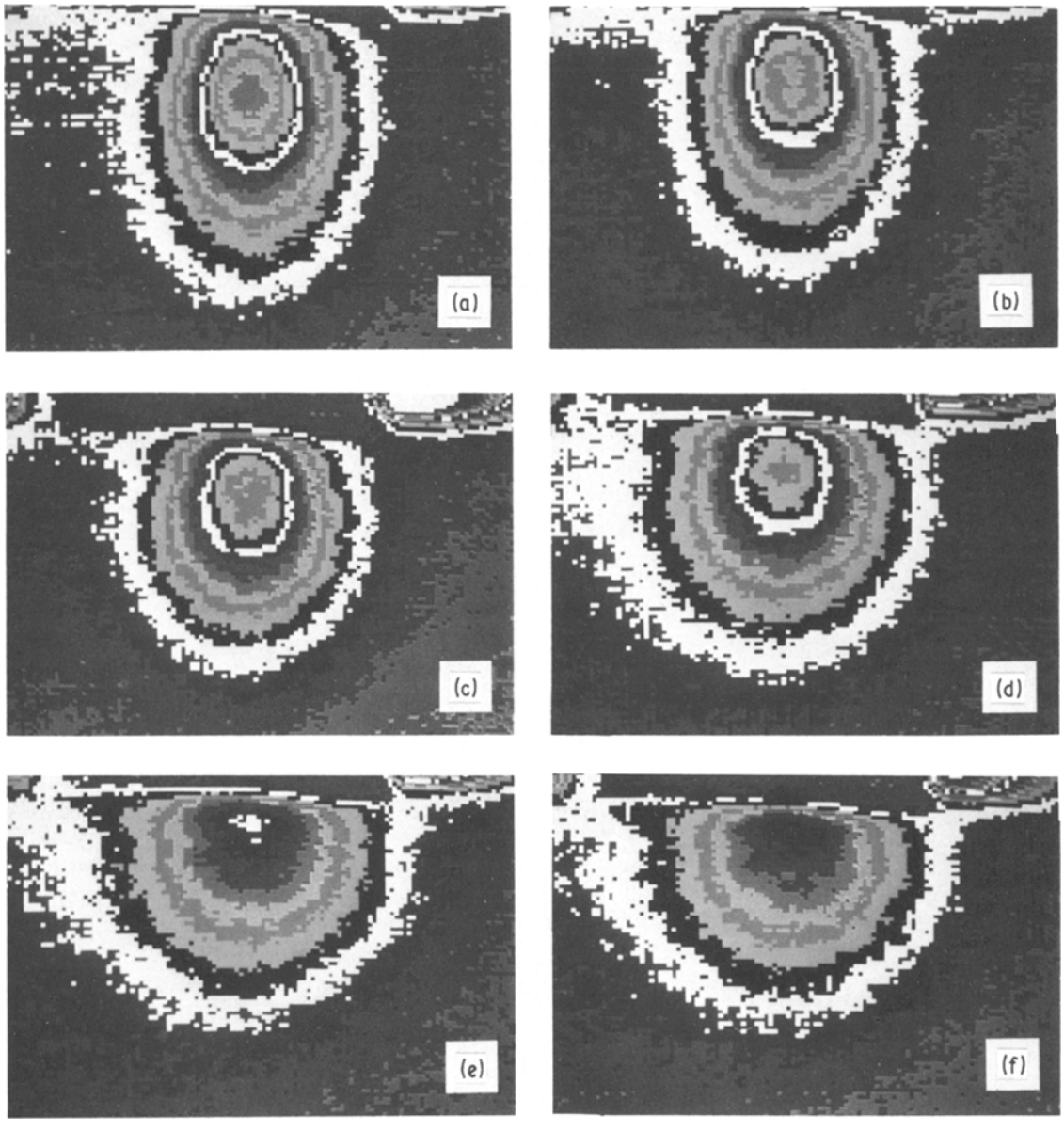

Figure 4 Craze SAXS patterns during step-wise unloading at the following surface strains: (a) maximum strain, 3.03%, (b) 2.48%, (c) 1.93%, (d) 1.34%,. (e) 0.83%, (f) 0.28%.

measured by a slit scan over the fibril streak. The invariant Q is defined by

$$Q = 2\pi \int_0^\infty si(s)\,ds \qquad (1)$$

For a two-phase system such as a craze, Q must be given by

$$Q = (\Delta\varrho)^2 v_f V(1 - v_f) \qquad (2)$$

where $\Delta\varrho$ is the electron density between the fibrils and their surroundings. Therefore

$$Q^0/Q = (1 - v_f^0)/(1 - v_f) \qquad (3)$$

where the superscript o denotes the loaded craze. From TEM measurements [22–24] $v_f^0 = 0.25$ so that the measurements of Q allow us to measure v_f at each strain. These measurements show that v_f abruptly increases below a surface strain of 1.3%. Above and below this strain no changes could be resolved. The results, shown in Table I, indicate that v_f increases from 0.25 above this strain to 0.40 below it.

For a two-phase system an analysis originally due to Porod [27–29] shows that at large scattering angles,

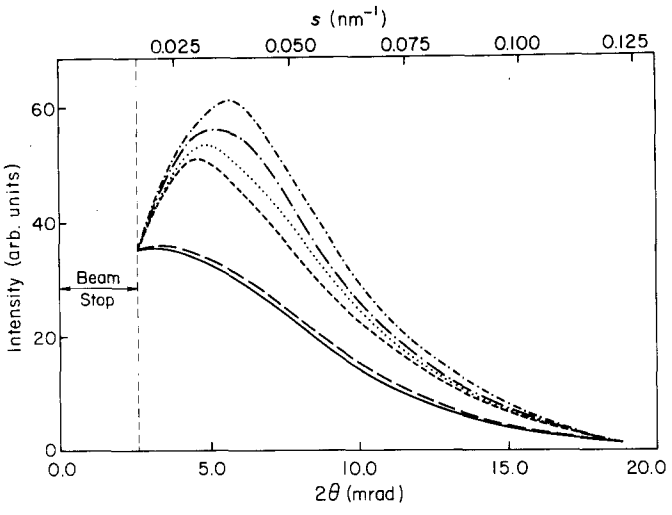

Figure 5 Longitudinal line scan along the fibril scattering streak during step-wise unloading. -·-·- surface strain = 3.03%; —·— = 2.48%; ····· = 1.93%; ---- = 1.38%; —— = 0.83%; ——— = 0.28%.

$$i(s) = K/s^3 \quad (4)$$

where K is a constant. We have determined that the Porod law is obeyed by the SAXS from craze microstructures and have extracted values of Q/K from the SAXS patterns using the image analyser. The mean fibril diameter can be found from [8, 16]

$$D = Q/[\pi^3(1 - v_f)K] \quad (5)$$

These values are also shown in Table I. The mean fibril diameter obtained for the fully loaded crazes, 6.3 nm, is in excellent agreement with the 6 nm measured previously for PS [8]. Decreasing the load causes an increase in the mean diameter of the load bearing fibrils to 7.7 nm. Such an increase is to be expected as the highly oriented molecules in the fibrils are allowed to relax. Nevertheless, this increase is not quite sufficient to account for the increase in v_f on unloading (it predicts that v_f increases only to 0.37). Hence unloading must also cause buckling of the fibrils. The predicted fibril buckling and misorientation is confirmed by Fig. 6 which shows circumferential scans performed at a fixed scattering angle of 10 mrad at several strains during the unloading. Although during the unloading a progressive increase in the misorientation of the fibrils is observed, there is also an abrupt increase in misorientation below a strain of 1.3%. It is likely that the initial buckling is associated with smaller diameter fibrils present while below a strain of 1.3% the fibril structure has collapsed, due to the onset of compressive forces produced by the elastically deformed polymer glass surrounding the crazes. The fact that the collapse of crazes during unloading occurs only at relatively low strains is in accord with the direct craze strain measurements of Kambour and Kopp [25] on dried ethanol crazes in polycarbonate as well as the evidence from the stress–strain hysteresis loops during fatigue of polymers which deform predominantly by crazing [30, 31].

TABLE I

Surface strain (%)	v_f	D (nm)
> 1.3	0.25	6.3
< 1.3	0.40	7.7

The changes observed in the fibril scattering are dependent on the frequency and temperature of the fatigue experiment [8]. At extremely low frequencies or high temperatures, there is relaxation of the stress in the bulk glass which is the cause of the compression of the fibrils. At the frequency and temperature of stepwise loading of our experiment, the initial craze microstructure is fully recoverable on reloading. At higher frequencies, or after a larger number of cycles, full recovery is not achieved.

Fig. 7 displays a longitudinal scan illustrating the appreciable increase in fibril scattering after a 10 cycle loading and unloading sequence at 0.6 Hz. It seems unlikely that the corresponding increase in Q is due to an increase in v_f, which would be implied by Equation 2 if V were constant. If anything v_f should decrease as fibrils break and retract in the craze. The only logical

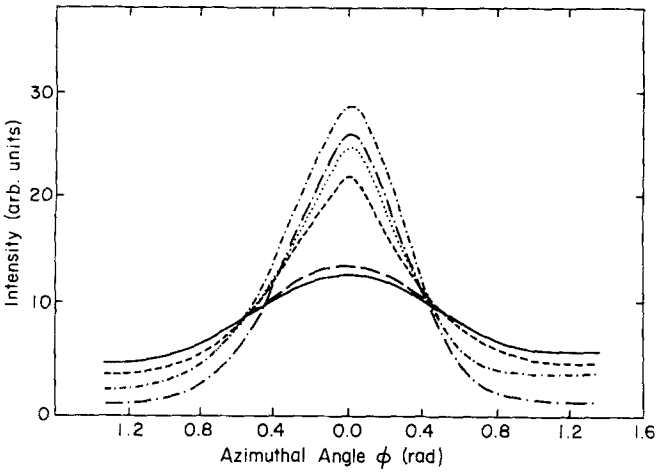

Figure 6 Circumferential line scans across the fibril scattering streak during step-wise unloading. –·–·– surface strain = 3.03%; —·— = 2.48%; ····· = 1.93%; ——— = 1.38%; — — — = 0.83%; —— = 0.28%. The broadening of the diffraction streak during unloading indicates a misorientation of the fibrils.

reason for the increase in Q and $i(s)$ is an increase in $v_f V$, the volume of polymer material in the craze. This volume would increase if more polymer were drawn into the craze each cycle, or if new crazes nucleate. Drawing of more polymer into crazes is known to be the mechanism of air craze widening during unidirectional loading [22–24]. It seems likely that this behaviour results from the viscoelastic response of the polymer fibrils themselves. They retract during the unloading portion of the cycle but do not instantly regain their fully stretched length upon reloading. The maximum stress on the fibrils is then larger than would be achieved under slower loading and hence more polymer is drawn into the fibrils (and/or new crazes would be nucleated) that would not be if the strain were held constant.

Clearly irreversible changes in the shape of the pattern also occur. The increased intensity in Fig. 7 occurs disproportionately at the smaller angles, which implies either that the new fibrils which are drawn are larger than the old ones or that some of the smaller fibrils in the craze break. That the latter is a strong possibility is demonstrated by the results of circumferential scans at the maximum load before and after the same 10 cycle fatigue sequence (Fig. 8). The broadening of the fibril diffraction streak after the sequence implies increased misorientation of the fibrils. Such misorientation is expected if a certain number of fibrils break during the fatigue sequence and thereafter adopt a more nearly random orientation. This result also holds out the possibility that real time SAXS may be useful in detecting early signs of damage in crazes during either fatigue or unidirectional loading.

4. Conclusion

This paper demonstrates that real time small-

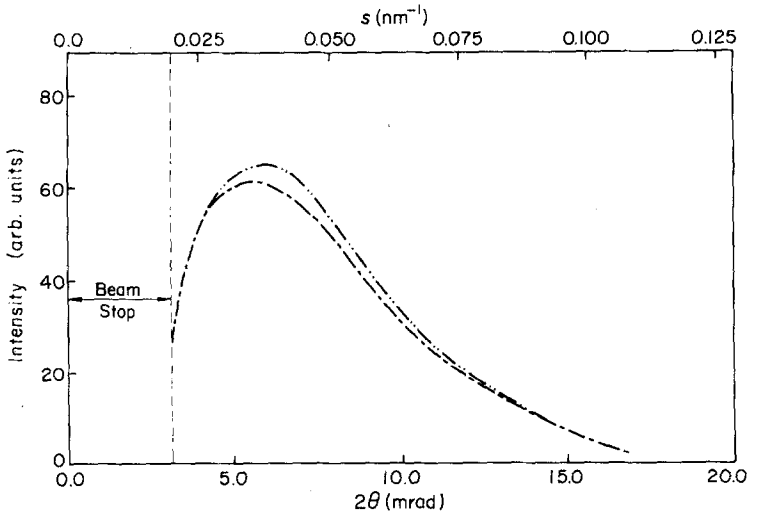

Figure 7 Longitudinal line scan of the fibril scattering streak at maximum load before (— — —) and after (— · · —) a 10 cycle fatigue loading and unloading sequence.

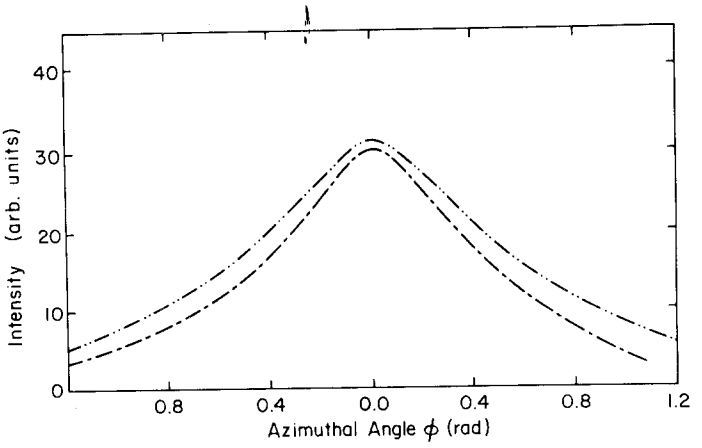

Figure 8 Circumferential line scans of the fibril scattering streak at maximum load before (——) and after (— · · —) a 10 cycle fatigue loading and unloading sequence at 0.6 Hz.

angle X-ray scattering is a powerful tool for observing changes in craze microstructure during deformation. The deformation of the craze fibrils themselves may be followed through measurements of the mean fibril diameter and fibril misorientation. The relative volume of craze matter can be determined and from it the closure of the craze surfaces and the increase in the fibril volume fraction on unloading. Absolute intensity measurements will allow one to measure the absolute volume of craze matter in the beam. From this parameter the overall strain due to crazing can be computed. Finally there is the possibility of following the failure of the craze fibrils themselves by monitoring the fibril misorientation at the point of maximum load in the fatigue cycle. Such measurements seem the only way at present to detect fibril failure well before fast crack propagation and specimen fracture.

Acknowledgements

Financial support for this research was provided by the NSF–DMR Polymers Program under Grant no. DMR-81231233 to H. R. Brown, while he was at Case-Western Reserve University, and Grant no. DMR-7919828 to E. J. Kramer at Cornell. The work also benefited from the use of the facilities of the Cornell Materials Science Center which is funded by the National Science Foundation, DMR-MRL, which also supported P. J. Mills as a post-doctoral fellow. The authors greatly appreciate the assistance given to us by all the CHESS staff whilst performing the experiments, in particular D. H. Bilderback and M. Caffrey whose detector system made the work possible. We also appreciate the assistance of W. W. Webb and D. Gross in allowing us to use their image analyser.

References

1. R. W. HERTZBERG and J. A. MANSON, "Fatigue of Engineering Plastics" (Academic Press, New York, 1980).
2. E. H. ANDREWS, "Fracture of Polymers" (American Elsevier, New York, 1968).
3. J. G. WILLIAMS, *J. Mater. Sci.* **12** (1977) 2525.
4. M. J. DOYLE, *ibid.* **18** (1983) 687.
5. M. D. SKIBO, R. W. HERTZBERG, J. A. MANSON and S. L. KIM, *ibid.* **12** (1977) 531.
6. J. A. SAUER and G. C. RICHARDSON, *Int. J. Fract.* **16** (1980) 499.
7. W. DÖLL, *Adv. Polym. Sci.* **52/3** (1983) 106.
8. H. R. BROWN and E. J. KRAMER, *J. Macromol. Sci. Phys.* **B19** (1981) 487.
9. W. S. ROTHWELL, R. H. MARTINSON and R. L. GORMAN, *Appl. Phys. Lett.* **42** (1983) 422.
10. D. G. LeGRAND, R. P. KAMBOUR and W. R. HAAF, *J. Polym. Sci. Polym. Phys. A2* **10** (1972) 1565.
11. T. R. STEGER and L. E. NIELSEN, *ibid.* **16** (1978) 613.
12. E. PAREDES and E. W. FISCHER, *Makromol. Chem.* **180** (1979) 2707.
13. M. DETTENMAIER and H. H. KAUSCH, *Polymer* **21** (1980) 1232.
14. E. PAREDES and E. W. FISCHER, *J. Polym. Sci. Polym. Phys.* **20** (1982) 929.
15. M. DETTENMAIER, *Adv. Polym. Sci.* **52/53** (1983) 84.
16. P. A. WESTBROOK, J. F. FELLERS, R. W. HENDRICKS and J. S. LIN, *J. Polym. Sci. Polym. Phys.* **21** (1983) 969.
17. P. A. WESTBROOK, J. F. FELLERS, M. CAKMAK, J. S. LIN and R. W. HENDRICKS, *ibid.* **21** (1983) 1913.
18. H. H. BROWN, Y. SINDONI, E. J. KRAMER and P. J. MILLS, *Polym. Eng. Sci.* **24** (1984) 825.
19. R. P. KAMBOUR and S. A. HOLIK, *J. Polym. Sci. A2* **7** (1969) 1393.
20. P. BEAHAN, M. BEVIS and D. HULL, *Phil. Mag.* **24** (1971) 1267.

21. S. WELLINGHOFF and E. BAER, *J. Macromol. Sci. (B)* **11** (1975) 367.
22. B. D. LAUTERWASSER and E. J. KRAMER, *Phil. Mag. (A)* **39** (1979) 469.
23. H. R. BROWN, *J. Mater. Sci.* **14** (1979) 237.
24. E. J. KRAMER, *Adv. Polym. Sci.* **52/53** (1983) 1.
25. R. P. KAMBOUR and R. W. KOPP, *J. Polym. Sci. Polym. Phys. A2* **7** (1969) 183.
26. H. R. BROWN and I. M. WARD, *Polymer* **14** (1973) 469.
27. G. POROD, *Kolloid Z.* **124** (1951) 83.
28. *Idem, ibid.* **125** (1952) 51.
29. P. DEBYE, H. R. ANDERSON Jr and H. BRUMBERGER, *J. Appl. Phys.* **28** (1957) 679.
30. P. BEARDMORE and S. RABINOWITZ, *Appl. Polym. Symp.* **24** (1974) 25.
31. J. A. SAUER and C. C. CHEN, *Adv. Polym. Sci.* **52/53** (1983) 169.

Received 12 December 1984
and accepted 15 January 1985